HHS Public Access

Author manuscript

Analyst. Author manuscript; available in PMC 2015 September 21.

Published in final edited form as:

Analyst. 2014 September 21; 139(18): 4401–4410. doi:10.1039/c4an00990h.

Enhancing Magnetic Resonance Imaging with Contrast Agents for Ultra-High Field Strengths

Akhila N. W. Kuda-Wedagedara[a] and **Matthew J. Allen**[a]

Matthew J. Allen: mallen@chem.wayne.edu

[a]Department of Chemistry, Wayne State University, 5101 Cass Avenue, Detroit, MI 48202, USA. Fax: 1 313 577 8822; Tel: 1 313 577 2070

Abstract

Contrast agents are diagnostic tools that often complement magnetic resonance imaging. At ultra-high field strengths (≥7 T), magnetic resonance imaging is capable of generating desirable high signal-to-noise ratios, but clinically available contrast agents are less effective at ultra-high field strengths relative to lower fields. This gap in effectiveness demands the development of contrast agents for ultra-high field strengths. In this minireview, we summarize contrast agents reported during the last three years that focused on ultra-high field strengths.

Introduction

Magnetic resonance imaging (MRI) is a non-invasive technique that can map the relaxation rates of water protons in a magnetic field to generate images. Common clinical magnetic field strengths are 1.5 and 3 T, but the number of higher field strength systems increases each year. Over forty clinical and preclinical 7 T MRI scanners are available in the United States, and many higher field strength scanners (≥7 T) are used in preclinical research.[1–4]

Magnetic fields at or above 7 T are classified as ultra-high field strengths, and the use of 7 T magnets for clinical MRI has been reported.[5–8] There is a strong urge to use ultra-high field MRI scanners because of the advantages that can be gained with ultra-high field strengths relative to lower field strengths, including high signal-to-noise ratios, high spatial resolution, short acquisition times, and the ability to use low sensitivity nuclei other than ^{1}H (including ^{19}F, ^{13}C, ^{23}Na, and ^{31}P).[2–4] These advantages are demonstrated by the increased amount of information that can be gained from MR images at ultra-high field strengths compared to lower field strengths (Fig. 1).

Obtaining high quality MR images (high contrast-to-noise ratios) is critical in diagnosing diseases, but increases in magnetic field strength alone are not always sufficient to obtain images with high contrast-to-noise ratios. High contrast-to-noise ratios often can be achieved using paramagnetic metal complexes called contrast agents.[9] For example, complexes **1–6** shown in Fig. 2 are clinically approved contrast agents that are used to improve contrast-to-noise ratios in MR images in approximately half of all clinical scans.[9–12] Contrast agents influence both longitudinal ($1/T_1$) and transverse ($1/T_2$) relaxation rates, and clinically approved contrast agents can be categorized into two types of agents: those with T_1/T_2 ratios close to one (T_1-shortening or positive agents) and those with T_1/T_2

ratios ≥6 (T_2-shortening or negative agents).[12,13] Both types of contrast agents usually contain paramagnetic metal ions that increase the relaxation rates ($1/T_1$ and $1/T_2$) of the protons of the surrounding molecules, but current clinical contrast agents are less effective at ultra-high magnetic fields than at lower fields (Table 1).[14–16] Note: care should be taken to only compare relaxivity values reported at the same temperature and in the same solvent.

Because of the decrease in relaxivity with increasing field strength, a great deal of research has focused on modifying Gd^{III}-based agents to increase relaxivity at ultra-high field strengths. Additionally, other types of contrast agents have been studied to meet the need of efficient contrast agents at ultra-high fields. Much of this work has been reviewed,[13,17–25] and this review is intended to describe both Gd^{III}-based and non-Gd^{III}-based strategies to influence contrast in ultra-high field MRI from the last three years with a focus on discrete molecules. For reviews focused on nanoparticles, we suggest a few other reviews.[26–31] This review is divided into four sections: (1) optimization of Gd^{III}-based agents; (2) Eu^{II}-containing cryptates as T_1-shortening agents; (3) ^{19}F-MRI agents; and (4) chemical exchange saturation transfer agents.

(1) Optimization of Gd^{III}-Based Agents

Molecular parameters that influence the relaxivity of T_1-shortening agents include the number of coordinated water molecules and the electronic relaxation, water-exchange, and rotational correlation rates. This review does not go into detail regarding these properties because they have been described elsewhere;[34–37] however, at field strengths higher than 1.5 T, the electronic relaxation rates do not contribute significantly to relaxivity,[37] but water-exchange and rotational correlation rates need to be optimized as a function of field strength to achieve fast longitudinal relaxation rates of the protons of the surrounding molecules.[36] Another parameter that influences relaxivity is the number of coordinated water molecules. Increasing this number usually increases relaxation rates but often leads to complexes with lowered kinetic stabilities.[38] However, incorporation of multiple complexes into one molecule is a way to influence the rotational correlation rate and the number of coordinated water molecules without necessarily sacrificing kinetic stability.

Apart from the number of coordinated water molecules, the relaxivities of clinically used T_1-shortening contrast agents (**1**–**6**, Fig. 2) are limited by fast rotational correlation rates (water-exchange rates do not play a large role in relaxivity at ultra-high fields for Gd^{III}-based T_1-shortening agents until rotational correlation rates have been optimized);[13] therefore, optimizing rotational correlation rates is essential to achieve high relaxivity. To slow rotational correlation rates, conjugation to relatively large molecules such as proteins has been studied (the use of macromolecules also influences biodistribution and half-life in vivo).[39–41] Although macromolecule-conjugation is effective at lower field strengths (≤3 T), this strategy causes too much slowing of the rotational correlation rates and negatively impacts relaxivity at ultra-high field strengths. To achieve the best relaxivity above 3 T, it is necessary to bring the rotational correlation rate to an intermediate range (2.5×10^8 to 2×10^9 s^{-1}).[36,38] Rotational correlation rate is influenced by the molecular weight and flexibility of a complex; therefore, by slightly increasing the steric bulk or by linking

multiple Gd^{III}-containing complexes together, the rotational correlation rate can be targeted to the desired region for a specific field strength.[13]

Meade and co-workers reported the conjugation of multiple Gd^{III}-containing complexes via 5-(2,4,6-triethenylphenoxy)pentanoic acid to produce trimeric complex **7** with rigid triazole linkers to bring the rotational correlation rate to an intermediate range (Fig. 3).[42] Complex **7** displays a 170% higher per-Gd relaxivity (Table 2) at ultra-high fields compared to unconjugated complex **8** due to the decrease in rotational correlation rate from 2×10^{10} to 1.7×10^{9} s^{-1}.[42]

Another example of optimizing rotational correlation rate was reported by Yang and co-workers.[43] They metalated the apo proteins ProCA1 and polyethylenglycol (PEG)-conjugated ProCA1 with Gd^{III} (Fig. 4). The relaxivities of PEGylated Gd^{III}-containing ProCA1 proteins are higher at ultra-high field strengths than non-PEGylated Gd^{III}-containing ProCA1 (Fig. 4B) and Gd^{III}-DTPA due to the slowing of rotational correlation rate and the increase in water-coordination number (water-coordination numbers: Gd^{III}-DTPA = 1.1, Gd^{III}-containing ProCA1 = 2.4, and Gd^{III}-containing PEGylated ProCA1 = 3.0).

In addition to conjugation of multiple Gd^{III}-containing units or incorporation of Gd^{III} ions into proteins, conjugation of small molecules to Gd^{III}-containing complexes is a method to increase relaxivity at ultra-high field strengths (Fig. 3, Table 2). Wang and co-workers reported myelin-specific Gd^{III}-based contrast agents **9** and **10** that have higher relaxivities than **1** (3.9 mM^{-1} s^{-1} at 9.4 T and 25 °C) or **2** (4.1 mM^{-1} s^{-1} at 9.4 T and 25 °C) at ultra-high field strengths due to the increase in molecular weight resulting from conjugation with stilbene or coumarin derivatives (Table 2).[44,45] Chuang, Yang, and co-workers reported complex **11** as a potential tumour-targeting contrast agent that displays higher relaxivities than clinically approved contrast agents **1** or **2** at 9.4 T (Table 2).[46] Hagberg and co-workers reported a calcium ion sensitive contrast agent **12** that increased the relaxivity from 2.9 to 6.5 mM^{-1} s^{-1} at 37 °C and at 7 T as a function of the concentration of Ca^{2+}.[51] Caravan and co-workers reported Gd^{III}-DOTAla-based complexes **13–18** that have rotational rates (1.7×10^{9} to 6.7×10^{9} s^{-1}) and water-exchange rates that are near optimal at ultra-high field strengths.[47] Complexes **13**–**18** have higher relaxivities compared to clinically approved contrast agents **4** (3.0 mM^{-1} s^{-1} at 37 °C) and **5** (4.8 mM^{-1} s^{-1} at 37 °C) at 9.4 T (Table 1).[47] Bates and co-workers synthesized complexes **19** and **20** that display higher per-Gd relaxivities compared to clinically used contrast agents **1** and **2** at 9.4 T.[48] Complex **19** is seven coordinate (Gd^{III} usually has a coordination number of nine); therefore, two remaining coordination sites can be occupied by water molecules to produce a water-coordination number of two. A higher water-coordination number and larger molecular weight caused complex **19** to have a higher relaxivity than clinically approved contrast agents. However, adjacent water-coordination sites are prone to coordination by bidentate anions like carbonates and phosphates leading to low relaxivities in biologically relevant media.[52] Complex **20**, relative to **19**, contains an octadentate ligand leaving only one site for water, but due to the higher molecular weight, complex **20** displays a slower rotational correlation rate leading to higher relaxivity than clinical contrast agents at ultra-high fields. Angelovski and co-workers reported a series of Gd^{III}-based complexes (**21**–**24**) that display

higher relaxivities than clinically approved contrast agents **1** and **2** at 7 T and 25 °C (Table 2).[49]

The examples in this section demonstrate the influence of rotational correlation rate and the number of coordinated water molecules on relaxivity at ultra-high field strengths. Although these examples show increases in relaxivity at ultra-high fields compared to clinically approved T_1-shortening contrast agents, the relaxivities per metal ion for complexes **7**–**24** are only slightly larger than the relaxivities of clinically approved T_1-shortening contrast agents at ultra-high field strengths and 37 °C. This small increase has generated interest in alternatives to Gd^{III}-based contrast agents, and these agents are described in the remaining sections of this review.

(2) Eu^{II}-Containing Cryptates as T_1-Shortening Agents

Eu^{II}-containing cryptates have been explored as an alternate to Gd^{III}-containing contrast agents. Eu^{II} is isoelectronic with Gd^{III}, and the molecular parameters that influence the relaxivity of Gd^{III} influence Eu^{II} in similar fashion.[53] However, the larger radius (117 pm for Eu^{II} vs 93.8 pm for Gd^{III})[54] and lower charge of Eu^{II} allow the ion to have faster water-exchange rates than Gd^{III}.[55] Further, Eu^{II}-containing cryptates have two coordinated water molecules because Eu^{II} is large enough to have a coordination number of ten.[55]

Allen and co-workers reported a series of Eu^{II}-containing cryptates **25**–**27** (Fig. 5) that are more efficient contrast agents than **2** (3.7 mM^{-1} s^{-1} at 7 T and 19 °C) at ultra-high field strengths (Table 2).[50] The higher relaxivities of Eu^{II}-containing cryptates relative to **2** at ultra-high fields are due to the ability to accommodate two water molecules in the inner sphere, the increase in water-exchange rates, and changes in rotational correlation rates compared to **2**.[50,56] The differences in relaxivities among different cryptates arise mainly from the changes in the rotational correlation rates that are proportional to molecular weight differences.[50] Eu^{II}-containing cryptates that display higher relaxivities than Gd^{III}-based contrast agents at ultra-high field strengths are potential alternatives to Gd^{III}-based contrast agents in T_1-weighted imaging. One of the current limitations of Eu^{II}-containing complexes is their tendency to oxidize to Eu^{III} in the presence of air. While some work has been done to overcome this effect,[57,58] further investigations are required to understand the *in vivo* outcomes of the oxidized products.

(3) ^{19}F-MRI Agents

^{19}F-MRI works similarly to ^{1}H-MRI, but instruments map the relaxation of ^{19}F (part of the contrast agent), as opposed to ^{1}H (part of the environment surrounding the contrast agent), to produce images. One advantage of using ^{19}F instead of ^{1}H is the lack of background signal (^{19}F is not found in appreciable amounts in humans outside of teeth).[59] The ^{19}F nuclei have 100% natural abundance and 83% NMR sensitivity relative to ^{1}H, making ^{19}F-MRI an active area of research.[59–62] Contrast enhancement with ^{19}F-MRI is increased with the use of ultra-high field strengths because signal intensity is proportional to field strength. This increase in signal intensity results in lower amounts of fluorinated agents being needed to obtain MR images (usually ^{19}F-MRI requires concentrations of ^{19}F to be in the millimolar range for imaging).[63] Because of the low sensitivity for detection of ^{19}F by MRI, two

strategies have been reported to increase the sensitivity of ^{19}F-MRI. The first strategy is to incorporate as many ^{19}F atoms into the structure as possible, and the other strategy is to incorporate a lanthanide ion to influence the relaxation rate of nearby ^{19}F nuclei.[63] Increases in relaxation rates also allow for faster acquisition rates in imaging.[64]

A series of ^{19}F-labeled lanthanide-based contrast agents (**28**–**32**, Fig. 6) were reported by Blamire and co-workers.[63] They used phosphonate-based 1,4,7,10-tetraazacyclododecane-1,4,7-triacetate (DO3A)-type ligands that were metalated with different lanthanide ions. Selection of the lanthanide ion and the imaging parameters were found to be key factors for using these agents for ultra-high field applications. Blamire and co-workers also reported that Dy^{III}-containing complex **29** provided the highest relaxation rates of the group at 4.7, 7.0, and 9.4 T (Table 3). Due to the high contrast gained from incorporation of Dy^{III}, micromolar concentrations (20 μM) of **29** were detectable in phantom images compared to the typical sensitivity of ^{19}F-MRI that is usually in the millimolar range.[63] Incorporation of lanthanide ions have been reported by Parker and co-workers with a phosphonate-based Dy^{III}-DO3A conjugated to chitosan (a linear polysaccharide) to result in complex **33** (Fig. 6) that shows comparable longitudinal relaxation rates to complex **29** at 4.7 and 9.4 T (Table 3).[65] Conjugation of chitosan improved the retention time of complex **33** *in vivo* leading to lower amounts of the contrast agent being needed for imaging.

Faber and co-workers reported complexes **34**–**37**.[66] Complexes **34** and **35** displayed higher relaxation rates (Table 3) and signal-to-noise ratios than complexes **36** and **37** at 9.4 T, leading to higher sensitivities. Kikuchi and co-workers reported contrast agents **38** and **39** that show decreased relaxation rates in the presence of enzymes.[67,68] Complexes **38** and **39** react with β-galactosidase and β-lactamase, respectively, resulting in detachment of the ^{19}F-containing moiety from the metal complex and a slowing of relaxation rates.

Contrast agents based on ^{19}F are important because of the near zero background signal and the high natural abundance of the ^{19}F nucleus. Ultra-high field strengths enhance the signal intensity of ^{19}F-based contrast agents, and ^{19}F-based agents are potentially useful in monitoring changes in biological environments, but the low sensitivity of ^{19}F-based agents limits their applicability and justifies further investigation in this area.

(4) Chemical Exchange Saturation Transfer Agents

In addition to T_1-weighted imaging used for ^{1}H and ^{19}F, another type of MRI experiment is chemical exchange saturation transfer (CEST) that uses proton transfer between two chemically distinct proton pools to produce images. In CEST, one pool is saturated by a radio frequency pulse, and chemical exchange of saturated protons with the bulk water decreases the signal intensity of the bulk water. The difference in the signal intensities before and after exchange can be mapped to produce images.[69] This imaging modality can be used to monitor changes in pH, temperature, and analyte concentration (anions and metal ions).[70,71] At ultra-high field strengths, high signal intensities for CEST can be achieved because, as with ^{19}F, signal intensity depends on the field strength.[24,69] Also, the separation between signals from CEST agents and bulk water increases with field strength. When the signal from a CEST agent is close (<5 ppm) to the bulk water signal, saturation pulses can excite protons in both pools decreasing the signal intensity (CEST effect) before the proton

exchange can take place. Interference with saturation frequency can be reduced by making the exchangeable pool appear farther from the bulk water signal (>5 ppm). Large frequency differences between the two pools also allow the use of relatively fast proton-exchange rates (for CEST agents, proton-exchange rates above 10^3 s^{-1} are considered fast) instead of the typically desired slow exchange rates (~2×10^3 s^{-1}).[72,73] This range of proton-exchange rates allows the use of CEST agents, including lanthanide-based paramagnetic CEST (PARACEST) agents that usually have intermediate to fast proton-exchange rates. PARACEST agents are mainly paramagnetic metal complexes that contain exchangeable protons. Because of the paramagnetic center, the exchangeable proton signal is shifted farther from the bulk water signal than in the case of CEST agents. This shift from the bulk water signal increases the sensitivity of the PARACEST agent. This shifting is especially important *in vivo* where there are many endogenous exchangeable protons. The following section describes the recent examples of CEST and PARACEST agents.

A series of thymidine-based (**40**–**43**, Fig. 7) CEST agents have been reported by Gilad and co-workers at 3 and 11.7 T.[74] For compounds **40** and **41**, distinguishable peaks (≥5 ppm from the bulk water signal) for amide protons were not observed at 3 T due to fast proton-exchange rates (≥3.7×10^3 s^{-1}), but at 11.7 T both **40** and **41** showed peaks distinct from the bulk water peaks. Compounds **42** and **43** showed signals for amide protons 5 ppm from the bulk water signal at both field strengths, but the peaks at 11.7 T were prominent because of the slow proton-exchange rate (≤1.7×10^3 s^{-1}).[74] CEST agents that show greater shifts from bulk water than thymidine-based agents have been reported by Pomper, McMahon, and co-workers.[75] These agents contain salicylic acid or its analogues (**44**–**50**, Fig. 7). Compounds **44**–**50** displayed shifts of 8.7–10.8 ppm from bulk water at 11.7 T at pH 7 and 37 °C. Compound **51** (Fig. 7) has been reported by Bulte, McMahon, and co-workers, and they showed that CEST activity detected with ^{19}F-NMR can be used to detect Ca^{2+} selectively in the presence of Mg^{2+} and Zn^{2+} (Ca^{2+} results in slow exchange rates compared to Mg^{2+} and Zn^{2+}).[76] The Ca^{2+}-containing complex shows 6.2 ppm shift from the free ligand. The fluorinated free ligands and metal-bound ligands were used as the exchangeable nuclei and ^{19}F-MRI was used to observe CEST activity.[76]

A series of Ln^{III}- and transition metal-based PARACEST complexes (**52**–**67**, Fig. 7) were reported by Morrow and co-workers.[71,77–83] Complex **52** displayed changes in CEST effect in response to the presence or absence of the biologically important anions lactate, citrate, and phosphate at 11.7 T and pH 6.5.[71] Complex **52** showed a chemical shift of 6 ppm from the bulk water signal in the CEST spectrum due to exchangeable alcohol protons. The addition of lactate and acetate shifted the peak to 7 ppm, and in the presence of citrate, the peak shifted to 8 ppm. Complexes **53** and **54** displayed changes in CEST effect in response to the interaction of phosphate diesters at neutral pH values.[77] Complex **53** showed a CEST signal around 5 ppm with respect to the bulk water when one equivalent of diethyl phosphate was added. Similarly, complex **54** displayed a CEST signal around 20 ppm with respect to bulk water when diethyl phosphate was added. Fe^{II}-containing PARACEST agents **55** and **56** displayed changes in CEST effect with respect to pH.[81] Complex **55** showed a CEST signal at 54 ppm, and the intensity of the peak decreased with increasing pH from 6.4 to 7.3 at 11.7 T and at 37 °C. The signal intensity of complex **56** at 50 ppm from

the bulk water increases in intensity with increasing pH from 6.8 to 7.6.[81] Complexes **58** and **61** showed 69 and 6 ppm shifts, respectively, from bulk water at 9.4 T.[78] The smaller shift observed with complex **61** compared to **58** was attributed to the slower proton-exchange rates of anilines compared to amides.

Complexes **59**, **62**, and **64** are Ni^{II}-containing PARACEST agents. The most intense CEST effect of the three was observed for complex **64** at 76 ppm from bulk water at 11.7 T.[79] Complexes **59** and **62** showed CEST effects at 76 and 72 ppm, respectively, from bulk water at 11.7 T, but the effects were 2–4-fold lower than that of complex **64**.[79] A series of Co^{II}-containing complexes **57**, **60**, **63**, **65**, and **67** have also been reported.[80,82] The redox active complex **67** was studied at 11.7 T as a potential probe to map *in vivo* oxygen levels.[80] Complex **67** with a CEST effect at 135 ppm from bulk water becomes CEST silent in the presence of oxygen.[80] Complexes **57**, **60**, **63**, and **65** displayed pH sensitive CEST effects in the pH range 6.5–7.5.[82] CEST signals for complexes **57** and **60** were at 45 and 32 ppm, respectively, and the signals for complex **65** were at –19 and 59 ppm.[82] Complex **63** displayed four CEST signals (112, 95, 54, and 45 ppm), and all shifts were measured at 11.7 T and 37 °C.[82] Complexes **64–66** were reported for their pH sensitive CEST effects between pH 6.5 and 7.7.[83] Complexes **64–66** displayed CEST signals at 72, 59, and 92 ppm, respectively, with CEST effects ranging from 25 to 39%.[83]

Kovacs and co-workers reported a Eu^{III}-containing PARACEST agent (**68**, Fig. 7) that can be activated by a redox reaction.[84] The complex contained nitroxide free radicals that slow the longitudinal relaxation rates of amide protons, but after oxidation in the presence of ascorbic acid, nitroxide radicals convert to nitroxide, resulting in an increase of the CEST effect to 20% at 9.4 T and 50 ppm from the bulk water.[84] Coman, Hyder, and co-workers reported a temperature-sensitive Eu^{III}-based PARACEST agent (**69**, Fig. 7) that enhanced the intensity of the CEST effect between 25 and 40 °C and decreased the intensity above 40 °C at 11.7 T due to increased water-exchange rate at high temperature.[85] Angelovski, Tóth, and co-workers reported calcium-ion-responsive PARACEST agents **70** and **71** that displayed a 60% CEST effect at 41 ppm and a 35% effect at −11 ppm, respectively, due to the exchange of amide protons in the absence of calcium ions (11.7 T, 37 °C, and pH 7.4).[86] The addition of calcium ions decreased the signal intensities due to the slowing of amide proton exchange. Durand, Tóth, and co-workers reported pH responsive PARACEST agents **72** and **73** that displayed CEST signals at about −25 ppm from bulk water at 11.7 T and 37 °C.[87] For complex **73**, a decrease in CEST effect from 65 to 15% was observed upon increasing the pH from 6.3 to 9.[87] Kotek and co-workers also reported pH responsive PARACEST agents.[88] Complexes **74** and **75** displayed changes in signal intensities over the pH range of 6–8. Complex **74** displayed two peaks at 19.5 and 34 ppm (25 °C and pH 7.67), and complex **75** displayed CEST signals at 42 and 89 ppm (25 °C and pH 7.4) at 7.05 T.[88]

Aime and co-workers reported Eu^{III}- and Yb^{III}-containing PARACEST agents **76** and **77** that displayed CEST signals at 20 ppm for the Eu^{III}-based agent and 71 and 99 ppm for the Yb^{III}-based agent (7 T, 20 °C, and pH 7.4) due to the exchanging hydroxyl protons.[89] Harris and co-workers reported PARACEST agents **78** and **79** that were linearly responsive to temperature changes in the range of 25 to 50 °C.[90] Complexes **78** and **79** showed CEST

signals at 9.4 T of 17 and 30 ppm, respectively, at 25 °C for the $S = 0$ state; and those signals shifted to 23 and 50 ppm at 50 °C corresponding to the $S = 2$ state.[90] Pagel and co-workers reported complexes **80**–**82** that are enzyme-responsive as well as pH responsive complex **83**.[91–94] Complex **80** reacts with esterases to produce hydrocourmarins and amine-functionalized metal complexes that in turn produce a CEST signal at 12 ppm (14 T, 37 °C, and pH 7.4).[91] Complex **81** reacts with the enzyme transglutaminase to form a covalent bond between the metal complex and albumin, decreasing the CEST effect caused by albumin at 4.6 ppm and leading to the appearance of a new signal at −9.2 ppm (14 T, 37 °C, and pH 7.4).[92] Complex **82**, on the other hand, becomes CEST silent after reacting with the enzyme urokinase (before the enzyme reaction, the metal complex displays a signal at −54.1 ppm at 7.05 T and 37 °C).[93] Complex **83** displayed CEST signals at −9.8 and 9.75 ppm, and the ratio between the intensities of these signals changes linearly with respect to changes in pH between 6.0 and 7.6 (14 T and 38.3 °C).[94] Hudson and co-workers synthesized a series of PARACEST agents **84**–**87** to study the CEST effect.[95,96] The CEST effects of complexes **84**–**86** were greater than 18%, whereas the analogous Tm^{III}- and Dy^{III}-containing complexes produced CEST effects less than 18%.[95] Complex **87** also has been studied for its pH responsive CEST effect.[96] This complex produced a six-fold increase in CEST effect upon changing pH from 6.5 to 7.0 (9.4 T and 37 °C).[96]

As demonstrated by the examples in this section, CEST agents can be effectively used at ultra-high field strengths to monitor biologically relevant environmental changes. Although CEST agents are versatile in terms of monitoring changes in environments, they suffer from low sensitivity which is a prime area for research.

Summary and Conclusions

Ultra-high field strength MRI is capable of generating images with high signal-to-noise ratios potentially making detection of pathologies more accurate. Contrast agents have been used to achieve high contrast between pathologies and the surrounding environment, but clinically approved contrast agents are less efficient at ultra-high field strengths relative to low field strengths. Optimization of molecular parameters to increase the efficiency of Gd^{III}-based contrast agents at ultra-high fields and other non-Gd^{III}-based strategies have been reported and are being investigated by a number of research groups. There is opportunity for different types of contrast agents to be used in ultra-high field applications, but further research is needed for all of these strategies. A possible future for ultra-high field contrast agents will likely consist of a combination of Gd^{III}-based and the variety of non-Gd^{III}-based strategies covered in this review.

Acknowledgments

The authors acknowledge the National Institutes of Health (R01EB013663) for support and Levi Ekanger for assistance with Fig. 4.

References

1. Duyn JH. NeuroImage. 2012; 62:1241. [PubMed: 22063093]
2. Moser E, Stahlberg F, Ladd ME, Trattnig S. NMR Biomed. 2012; 25:695. [PubMed: 22102481]

3. Kraff O, Fischer A, Nagel AM, Mönninghoff C, Ladd ME. J Magn Reson Imaging. 201410.1002/jmri.24573
4. Moser E. World J Radiol. 2010; 2:37. [PubMed: 21160738]
5. Kollia K, Maderwald S, Putzki N, Schlamann M, Theysohn JM, Kraff O, Ladd ME, Frosting M, Wanke I. Am J Neuroradiol. 2009; 30:699. [PubMed: 19147714]
6. Beisteiner R, Robinson S, Wurnig M, Hilbert M, Merksa K, Rath J, Höllninger I, Kilinger N, Marosi C, Trattnig S, Geißler A. NeuroImage. 2011; 57:1015. [PubMed: 21620980]
7. Moenninghoff C, Maderwald S, Theysohn JM, Kraff O, Ladd ME, Hindy NE, van de Nes J, Frosting M, Wanke I. Eur Radiol. 2010; 20:704. [PubMed: 19763581]
8. van der Kolk AG, Hendrikse J, Zwanenburg JJM, Visser F, Luijten PR. Eur J Radiol. 2013; 82:708. [PubMed: 21937178]
9. Li D, Zheng J, Weinmann HJ. Radiology. 2001; 218:670. [PubMed: 11230638]
10. Huang S, Liu C, Dai G, Kim YR, Rosen BR. NeuroImage. 2009; 46:589. [PubMed: 19264139]
11. Villaraza AJL, Bumb A, Brechbiel MW. Chem Rev. 2010; 110:2921. [PubMed: 20067234]
12. Tu C, Osborne EA, Louie Y. Ann Biomed Eng. 2011; 39:1335. [PubMed: 21331662]
13. Helm L. Future Med Chem. 2010; 2:385. [PubMed: 21426173]
14. Hagberg GE, Sheffler K. Contrast Media Mol Imaging. 2013; 8:456. [PubMed: 24375901]
15. Richardson OC, Scott MLJ, Tanner SF, Waterton JC, Buckley DL. Magn Reson Med. 2012; 68:1234. [PubMed: 22161901]
16. Rosenberg JT, Kogot JM, Ridel C, Strouse GF, Grant SC. Proc Intl Soc Magn Reson Med. 2009; 17:921.
17. Xue S, Qiao J, Pu F, Cameron M, Yang JJ. Nanobiotechnol. 2013; 5:163.
18. Terreno E, Castelli DD, Viale A, Aime S. Chem Rev. 2010; 110:3019. [PubMed: 20415475]
19. Heffern MC, Matosziuk LM, Meade TJ. Chem Rev. 2014; 114:4496. [PubMed: 24328202]
20. Garcia J, Allen MJ. Eur J Inorg Chem. 2012; 2012:4550. [PubMed: 23049283]
21. Hsieh V, Jasanoff A. ACS Chem Neurosci. 2012; 3:593. [PubMed: 22896803]
22. Ahrens ET, Zhong J. NMR Biomed. 2013; 26:860. [PubMed: 23606473]
23. Chan KWY, Bulte JWM, McMahon MT. WIREs Nanomed Nanobiotechnol. 2014; 6:111.
24. Liu G, Song X, Chan KWY, McMahon MT. NMR Biomed. 2013; 26:810. [PubMed: 23303716]
25. Srinivas M, Heerschap A, Ahrens ET, Figdor CG, de Vries IJM. Trends Biotechnol. 2010; 28:363. [PubMed: 20427096]
26. Xu W, Kattel K, Park JY, Chang Y, Kim TJ, Lee GH. Phys Chem Chem Phys. 2012; 14:12687. [PubMed: 22885983]
27. Gallo J, Long NJ, Aboagye EO. Chem Soc Rev. 2013; 42:7816. [PubMed: 23788179]
28. Quentin LT, Hervé S, Marie-Hélène D. Nanotechnology Reviews. 2013; 2:125.
29. Castelli DD, Terreno E, Longo D, Aime S. NMR Biomed. 2013; 26:839. [PubMed: 23784956]
30. Shan L, Chopra A, Leung K, Eckelman WC, Menkens AE. J Nanopart Res. 2012; 14:1122.
31. Srikar R, Upendran A, Kannan R. WIREs Nanomed Nanobiotechnol. 2014; 6:245.
32. Rohrer M, Bauer H, Mintorovitch J, Requardt M, Weinmann HJ. Invest Radiol. 2005; 40:715. [PubMed: 16230904]
33. Noebauer-Huhmann IM, Szomolanyi P, Juras V, Kraff O, Ladd ME, Trattnig S. Invest Radiol. 2010; 45:554. [PubMed: 20697225]
34. Caravan P, Zhang Z. Eur J Inorg Chem. 2012; 1916
35. Manus LM, Strauch RC, Hung AH, Eckermann AL, Meade TJ. Anal Chem. 2012; 84:6278. [PubMed: 22624599]
36. Caravan P, Farrar CT, Frullano L, Uppal R. Contrast Media Mol Imaging. 2009; 4:89. [PubMed: 19177472]
37. Caravan P, Ellison JJ, McMurry TJ, Lauffer RB. Chem Rev. 1999; 99:2293. [PubMed: 11749483]
38. Polasek M, Caravan P. Inorg Chem. 2013; 52:4084. [PubMed: 23517079]
39. Bryson JM, Reineke JW, Reineke TM. Macromolecules. 2012; 45:8939. [PubMed: 23467737]

40. Kundu A, Peterlik AH, Krssak HM, Bytzek AK, Pashkunova-Martic I, Arion IVB, Helbich TH, Keppler BK. J Inorg Biochem. 2011; 105:250. [PubMed: 21194625]
41. Garimella PD, Datta A, Romanini DW, Raymond KN, Francis MB. J Am Chem Soc. 2011; 133:14704. [PubMed: 21800868]
42. Mastarone DJ, Harrison VSR, Eckermann AL, Parigi G, Luchinat C, Meade TJ. J Am Chem Soc. 2011; 133:5329. [PubMed: 21413801]
43. Li S, Jiang J, Zou J, Qiao J, Xue S, Wei L, Long R, Wang L, Castiblanco A, White N, Ngo J, Mao H, Liu ZR, Yang JJ. J Inorg Biochem. 2012; 107:111. [PubMed: 22178673]
44. Frullano L, Zhu J, Miller RH, Wang Y. J Med Chem. 2013; 56:1629. [PubMed: 23311333]
45. Frullano L, Wang C, Miller RH, Wang Y. J Am Chem Soc. 2011; 133:1611. [PubMed: 21265506]
46. Chandrasekharan P, Yong CX, Poh Z, He T, He Z, Liu S, Robins EG, Chuang KH, Yang CT. Biomaterials. 2012; 33:9225. [PubMed: 23026708]
47. Boros E, Polasek M, Zhang Z, Caravan P. J Am Chem Soc. 2012; 134:19858. [PubMed: 23157602]
48. Kittigowittana K, Yang C-T, Cheah WC, Chuang KH, Tuang CY, Chang Y-T, Golay X, Bates RW. Chem Med Chem. 2011; 6:781. [PubMed: 21433294]
49. Placidi MP, Engelmann J, Natrajan LS, Logothetis NK, Angelovsky G. Chem Commun. 2011; 47:11534.
50. Garcia J, Neelavalli J, Haacke EM, Allen MJ. Chem Commun. 2011; 47:12858.
51. Hagberg GE, Mamedov I, Power A, Beyerlein M, Merkle H, Kiselev VG, Dhingra K, Kubìček V, Angelovsky G, Logothetis NK. Contrast Media Mol Imaging. 2014; 9:71. [PubMed: 24470296]
52. Silvério S, Torres S, Martins AF, Martins JA, André JP, Helm L, Prata MIM, Santos AC, Geraldes CFGC. Dalton Trans. 2009:4656. [PubMed: 19513474]
53. Garcia J, Allen MJ. Inorg Chim Acta. 2012; 393:324.
54. Greenwood, NN.; Earnshaw, A. Chemistry of the Elements. 2. Elsevier; Butterworth-Heinmann, Burlington: 2005. p. 1233
55. Burai L, Scopelliti R, Tóth É. Chem Commun. 2002:2366.
56. Garcia J, Kuda-Wedagedara ANW, Allen MJ. Eur J Inorg Chem. 2012; 2012:2135. [PubMed: 22639543]
57. Gamage NDH, Mei Y, Garcia J, Allen MJ. Angew Chem Int Ed. 2010; 49:8923.
58. Gál M, Kielar F, Sokolová R, Ramešová S, Kolivoška V. Eur J Inorg Chem. 2013; 2013:3217.
59. Harvey P, Chalmers KH, Luca ED, Mishra A, Parker D. Chem Eur J. 2012; 18:8748. [PubMed: 22689478]
60. Matsushita H, Mizukami S, Mori Y, Sugihara F, Shirakawa M, Yoshioka Y, Kikuchi K. Chem Bio Chem. 2012; 13:1579.
61. Ruiz-Cabello J, Barnett BP, Bottomley PA, Bulte JWM. NMR Biomed. 2011; 24:114. [PubMed: 20842758]
62. Chen J, Lanza GM, Wickline SA. WIREs Nanomed Nanobiotechnol. 2010; 2:431.
63. Chalmers KH, Kenwright AM, Parker D, Blamire AM. Magn Reson Med. 2011; 66:931. [PubMed: 21381109]
64. Chalmers KH, Botta M, Parker D. Dalton Trans. 2011; 40:904. [PubMed: 21127807]
65. Luca ED, Harvey P, Chalmers KH, Mishra A, Senanayake PK, Wilson JI, Botta M, Fekete M, Blamire AM, Parker D. J Biol Inorg Chem. 2014; 19:215. [PubMed: 23955558]
66. Schmid F, Höltke C, Parker D, Faber C. Magn Reson Med. 2013; 69:1056. [PubMed: 22628001]
67. Mizukami S, Matsushita H, Takikawa R, Sugihara F, Shirakawa M, Kikuchi K. Chem Sci. 2011; 2:1151.
68. Matsushita H, Mizukami S, Mori Y, Sugihara F, Shirakawa M, Yoshika Y, Kikuchi K. Chem Bio Chem. 2012; 13:1579.
69. van Zijl PCM, Yadav NN. Magn Reson Med. 2011; 65:927. [PubMed: 21337419]
70. Dorazio SJ, Olatunde AO, Tsitovich PB, Morrow JR. J Biol Inorg Chem. 2014; 19:191. [PubMed: 24253281]

71. Hammell J, Buttarazzi L, Huang CH, Morrow JR. Inorg Chem. 2011; 50:4857. [PubMed: 21548563]
72. Vinogradov E, Sherry AD, Lenkinski RE. J Magn Reson. 2013; 229:155. [PubMed: 23273841]
73. Dula AN, Smith SA, Gore JC. J Neuroimaging. 2013; 23:526. [PubMed: 23402307]
74. Bar-Shir A, Liu G, Liang Y, Yadav NN, McMahon MT, Walczak P, Nimmagadda S, Pomper MG, Tallman KA, Greenberg MM, van Zijl PCM, Bulte JWM, Gilad AA. J Am Chem Soc. 2013; 135:1617. [PubMed: 23289583]
75. Yang X, Song X, Li Y, Liu G, Banerjee SR, Pomper MG, McMahon MT. Angew Chem Int Ed. 2013; 52:8116.
76. Bar-Shir A, Gilad AA, Chan KWY, Liu G, van Zijl PCM, Bulte JWM, McMahon MT. J Am Chem Soc. 2013; 135:12164. [PubMed: 23905693]
77. Huang CH, Hammell J, Ratnakar SJ, Sherry AD, Morrow JR. Inorg Chem. 2010; 49:5963. [PubMed: 20509631]
78. Dorazio SJ, Tsitovich PB, Siters KE, Spernyak JA, Morrow JR. J Am Chem Soc. 2011; 133:14154. [PubMed: 21838276]
79. Olatunde AO, Dorazio SJ, Spernyak JA, Morrow JR. J Am Chem Soc. 2012; 134:18503. [PubMed: 23102112]
80. Tsitovich PB, Spernyak JA, Morrow JR. Angew Chem Int Ed. 2013; 52:13997.
81. Dorazio SJ, Morrow JR. Inorg Chem. 2012; 51:7448. [PubMed: 22757664]
82. Dorazio SJ, Olatunde AO, Spernyak JA, Morrow J. Chem Commun. 2013; 49:10025.
83. Olatunde AO, Cox JM, Daddario MD, Spernyak JA, Benedict JB, Morrow JR. Inorg Chem. 201410.1021/ic5006083
84. Ratnakar SJ, Soesbe TC, Lumata LL, Do QN, Viswanathan S, Lin CY, Sherry AD, Kovacks Z. J Am Chem Soc. 2013; 135:14904. [PubMed: 24050192]
85. Coman D, Kiefer GE, Rothman DL, Sherry AD, Hyder F. NMR Biomed. 2011; 24:1216. [PubMed: 22020775]
86. Angelovski G, Chauvin T, Pohmann R, Logothetis NK, Tóth É. Bioorg Med Chem. 2011; 19:1097. [PubMed: 20691598]
87. Chauvin T, Torres S, Rosseto R, Kotek J, Badet B, Durand P, Tóth É. Chem Eur J. 2012; 18:1408. [PubMed: 22213022]
88. Krchová T, Kotek J, Jirák D, Havlíčková J, Císařová I, Hermann P. Dalton Trans. 2013; 42:15735. [PubMed: 24051547]
89. Ferrauto G, Castelli DD, Terreno E, Aime S. Magn Reson Med. 2013; 69:1703. [PubMed: 22837028]
90. Jeon IR, Park JG, Haney CR, Harris TD. Chem Sci. 2014; 5:2461.
91. Li Y, Sheth VR, Liu G, Pagel MD. Contrast Media Mol Imaging. 2011; 6:219. [PubMed: 21861282]
92. Hingorani DV, Randtke EA, Pagel MD. J Am Chem Soc. 2013; 135:6396. [PubMed: 23601132]
93. Yoo B, Sheth VR, Howison CM, Douglas MJK, Pineda CT, Maine EA, Baker AF, Pagel MD. Magn Reson Med. 2014; 71:1221. [PubMed: 23640714]
94. Sheth VR, Liu G, Li Y, Pagel MD. Contrast Media Mol Imaging. 2012; 7:26. [PubMed: 22344877]
95. Milne M, Chicas K, Li A, Bartha R, Hudson RHE. Org Biomol Chem. 2012; 10:287. [PubMed: 22069041]
96. Suchý M, Li AX, Milne M, Bartha R, Hudson RHE. Contrast Media Mol Imaging. 2012; 7:441. [PubMed: 22821878]

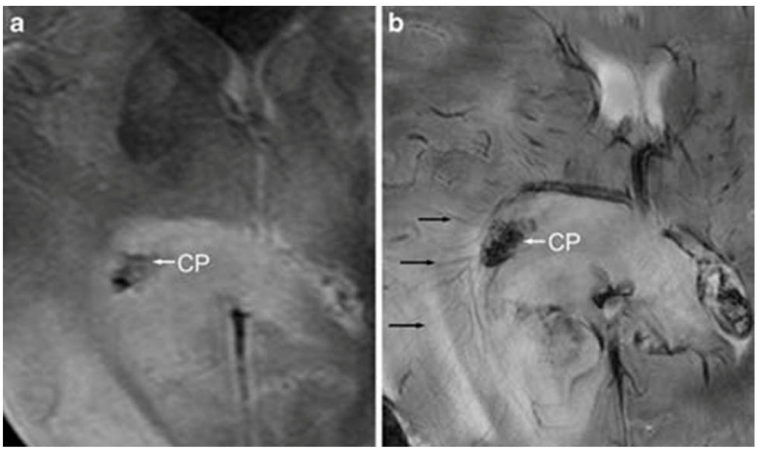

Fig. 1.

MR images of an axial slice of a human brain at (a) 1.5 and (b) 7 T. The image acquired at 7 T enables visualization of blood vessels (black arrows) and choroid plexus (CP, an abnormality in the right lobe) that are not clearly visible at 1.5 T.[7] Reprinted from C. Moenninghoff, S. Maderwald, J. M. Theysohn, O. Kraff, M. E. Ladd, N. El Hindy, J. van de Nes, M. Forsting and I. Wanke, Imaging of Adult Astrocytic Brain Tumours with 7 T MRI: Preliminary Results, *Eur. Radiol.*, 2010, **20**, 704–713, with kind permission from Springer Science and Business Media.

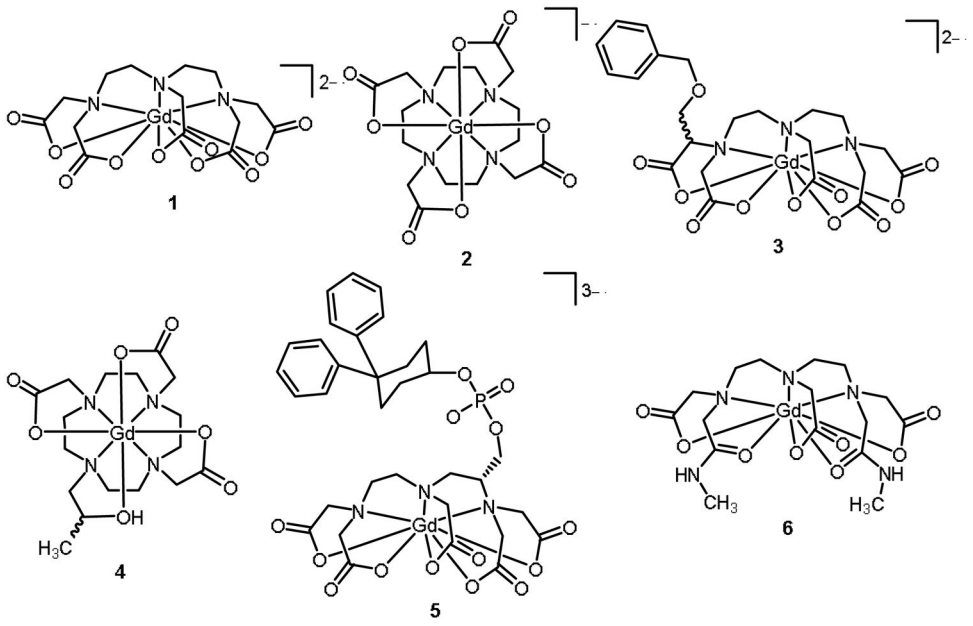

Fig. 2.

Clinically approved contrast agents: Gd^{III}-containing diethylenetriaminepentaacetate (DTPA), **1**; Gd^{III}-containing 1,4,7,10-tetraazacyclododecane-1,4,7,10-tetraacetate (DOTA), **2**; Gd^{III}-containing α-(benzyloxymethyl)diethylenetriaminepenta-acetate (BOPTA), **3**; Gd^{III}-DOTA derivative **4**; and Gd^{III}-DTPA derivatives **5** and **6** (coordinated water molecules and counter ions are not shown for clarity).

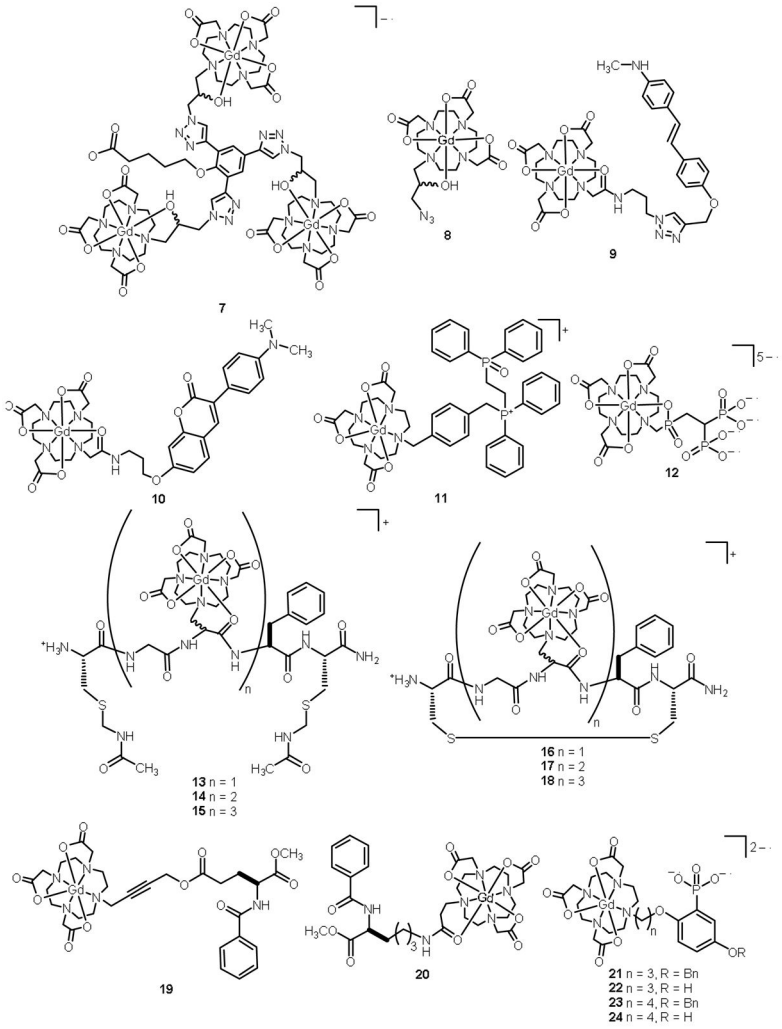

Fig. 3.

Chemical structures of contrast agents **7**–**24** (coordinated water molecules and counter ions are not shown for clarity).

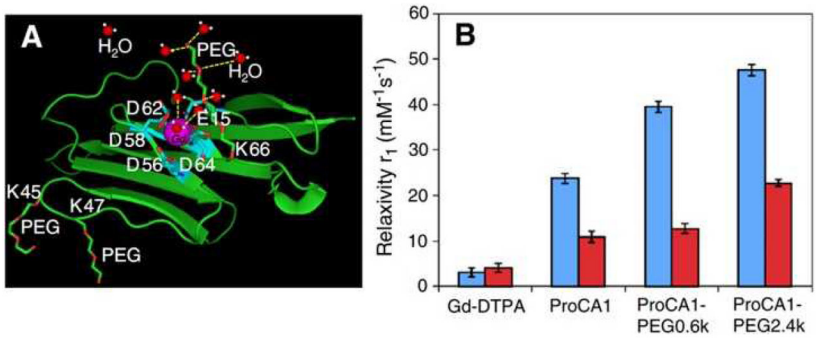

Fig. 4.

(A) Model of PEGylated ProCA1 metalated with Gd^{III} (pink: Gd^{III}; blue: metalation site; green: ProCA1; red and green: PEG; yellow and red: water); (B) Relaxivity values of ProCA1 and PEGylated-ProCA1 (blue at 3 T and red at 9.4 T). Reprinted from the *Journal of Inorganic Biochemistry*, **107**, S. Li, J. Jiang, J. Zou, J. Qiao, S. Xue, L. Wei, R. Long, L. Wang, A. Castiblanco, N. White, J. Ngo, H. Mao, Z.-R. Liu and J. J. Yang, PEGylation of Protein-Based MRI Contrast Agents Improves Relaxivities and Biocompatibilities, 111–118, Copyright 2013, with permission from Elsevier.

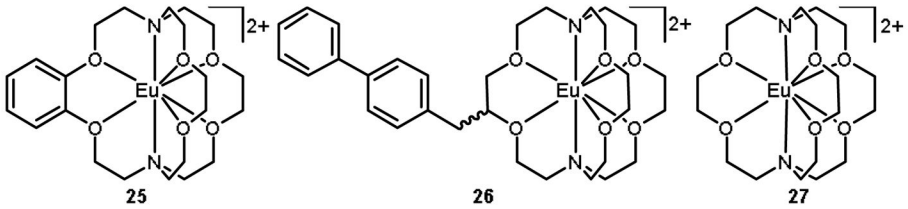

Fig. 5.

Eu^{II}-containing cryptates (**25**–**27**) (coordinated water molecules and counter ions are not shown for clarity).

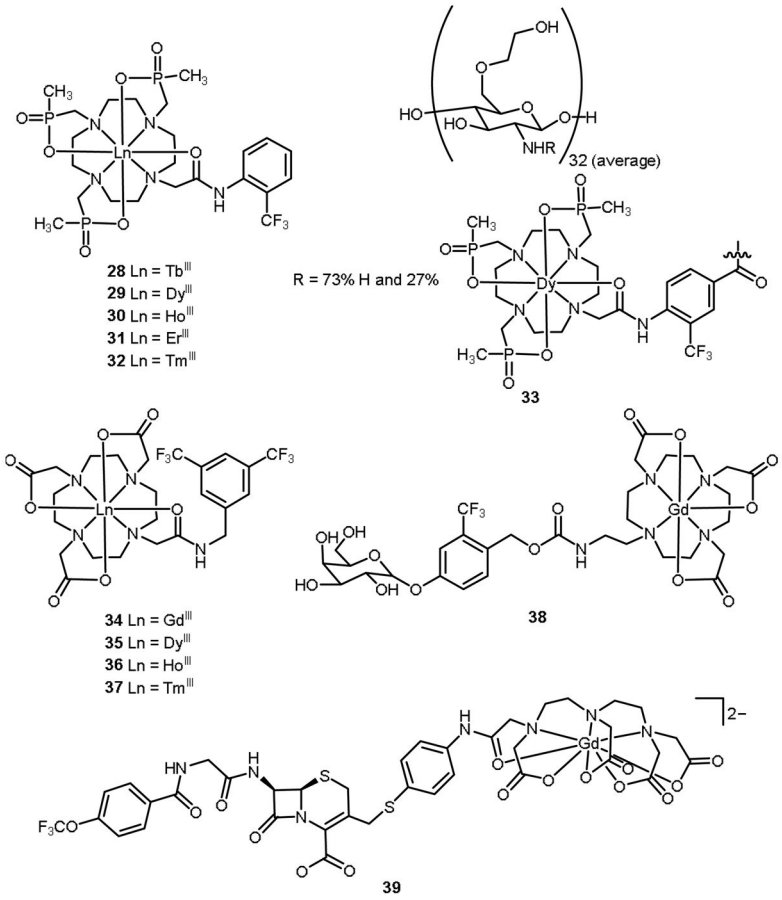

Fig. 6.
Ln^{III}-based contrast agents **28**–**39** for ^{19}F-MRI.

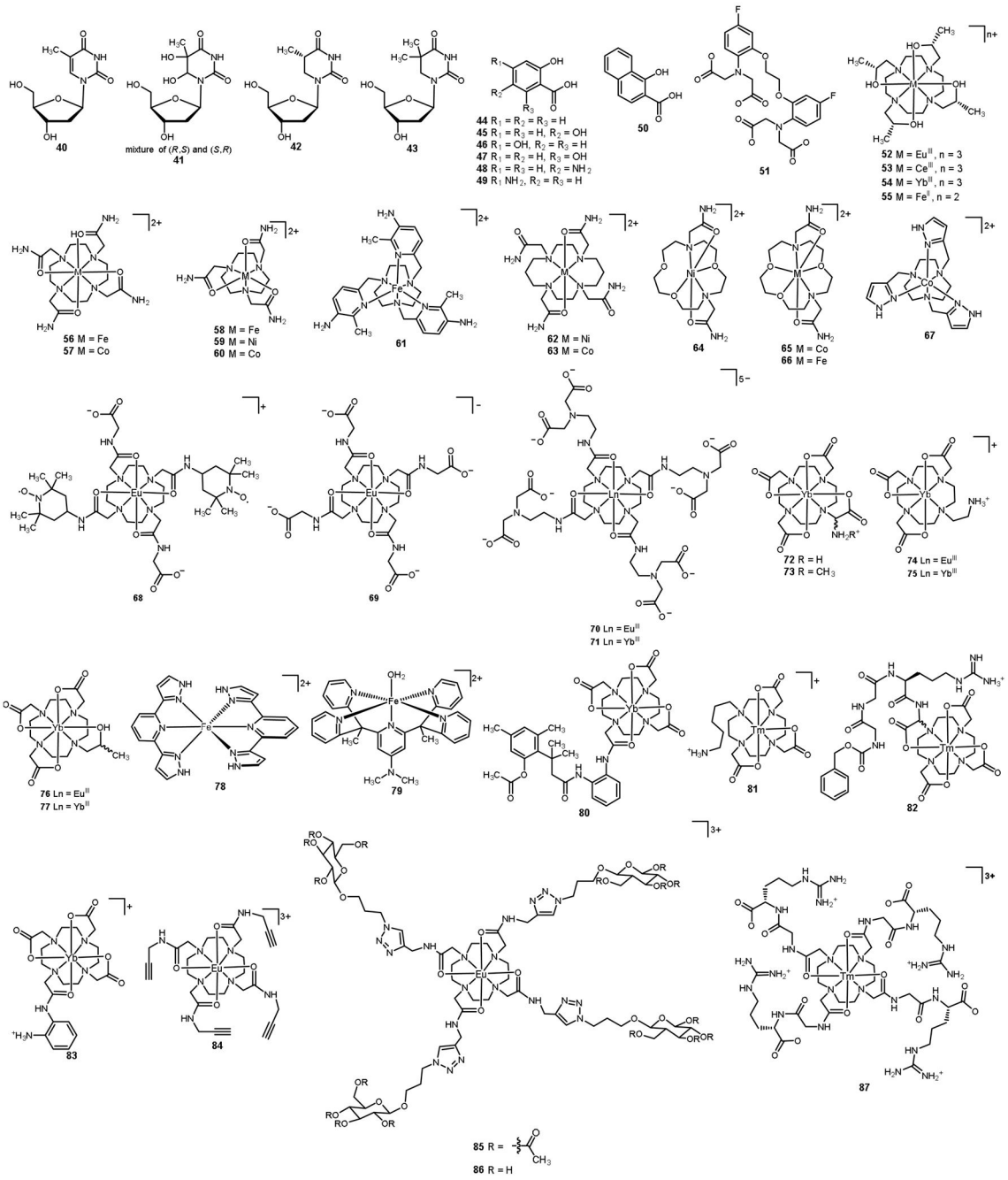

Fig. 7.

Structures of CEST (**40**–**51**) and PARACEST (**52**–**87**) agents. Some counter ions and coordinated water molecules have been omitted for clarity.

Table 1

Relaxivities (mM^{-1} s^{-1}) per-Gd^{III} of T_1-shortening contrast agents at 37 °C in blood.[32,33]

Complex	1.5 T	3 T	7 T
1	4.3	3.6	3.4
2	4.2	3.6	3.4
3	6.7	5.8	4.8
4	4.4	3.5	3.3
5	19	11.3	5.4
6	4.6	3.9	3.7

Table 2

Relaxivities (mM^{-1} s^{-1}) per-ion of T_1-shortening contrast agents at 37 ºC (unless otherwise noted) and 1.4, 3, 4.7, 7, 9.4, and 11.7 T.

Complex	1.4	3.0	4.7	7.0	9.4	11.7	Reference
7	15.4	–	–	–	4.8	–	42
8	3.05	–	–	–	2.79	–	42
9	5.1[a]	–	–	–	5.5[b]	–	44
10	5.1[a]	–	–	–	5.2[b]	–	45
11	–	–	–	–	5.9[c]	–	46
13	7.4	–	7	–	5.8	4.9	47
14	9.9	–	8.3	–	6.1	4.9	47
15	12.2	–	9	–	6.1	4.7	47
16	7.1	–	7.3	–	5.1	4.5	47
17	10.6	–	7.5	–	5.7	4.5	47
18	12.3	–	9.2	–	6.6	5.5	47
19	–	–	–	–	6.4[c]	–	48
20	–	–	–	–	5.4[c]	–	48
21	–	–	–	7.20[c]	–	–	49
22	–	–	–	7.33[c]	–	–	49
23	–	–	–	6.65[c]	–	–	49
24	–	–	–	5.23[c]	–	–	49
25	3.67	4.84[d]	–	6.47[e]	–	3.34	50
26	4.39	6.31[d]	–	7.17[e]	–	4.80	50
27	2.09	3.94[d]	–	5.01[e]	–	2.65	50

[a] 40 °C,

[b] 21 °C,

[c] 25 °C,

[d] 19.8 °C,

[e] 19 °C

Table 3

Longitudinal relaxation rates (s^{-1}) of ^{19}F-based contrast agents at 25 ºC and 4.7, 7, and 9.4 T.

Complex	4.7	7.0	9.4	Reference
28	84.0	113.0	146.6	63
29	103.8	143.9	184.8	63
30	58.1	88.0	120.1	63
31	71.1	90.9	108.9	63
32	46.6	56.4	63.3	63
33	108[a]	–	183[a]	65
34	–	–	694	66
35	–	–	160	66
36	–	–	69.9	66
37	–	–	130	66

[a] 22 °C